Cross section measurement of $\eta J/\psi$ and $\pi^0 J/\psi$ at $\sqrt{s} = 4.009$ GeV

Liu Zhiqing[1] and Yuan Changzheng[1]

[1]Institute of High Energy Physics, Beijing, 100049, China

(Dated: June 21, 2012)

Abstract

Using a 477 pb^{-1} data sample collected with the BESIII detector operating at the BEPCII storage ring at center-of-mass energy $\sqrt{s} = 4.009$ GeV, the production of $e^+e^- \to \eta J/\psi$ is observed for the first time with a statistical significance of greater than 10σ. The Born cross section is measured to be $(32.1 \pm 2.8 \pm 1.3)$ pb, where the first error is statistical and second systematic. Assuming the $\eta J/\psi$ signal is from a hadronic transition of the $\psi(4040)$, the transition rate is determined to be $\mathcal{B}(\psi(4040) \to \eta J/\psi) = (5.2 \pm 0.5 \pm 0.2 \pm 0.5) \times 10^{-3}$, where the first, the second, and the third errors are statistical, systematic, and uncertainty from $\psi(4040)$ resonant parameters, respectively. The production of $e^+e^- \to \pi^0 J/\psi$ is searched for, but no significant signal is observed, and $\mathcal{B}(\psi(4040) \to \pi^0 J/\psi) < 2.6 \times 10^{-4}$ is obtained at the 90% confidence level.

PACS numbers: 13.25.Gv, 13.40.Hq, 14.40.Pq

I. INTRODUCTION

The properties of excited 1^{--} charmonia above $D\bar{D}$ production threshold is of great interest but not well understood for several decades since their first observation [1]. By now, the well-established structures experimentally in the hadronic cross section are the $\psi(3770)$, the $\psi(4040)$, the $\psi(4160)$, and the $\psi(4415)$ [2]. Unlike the low-lying 1^{--} $c\bar{c}$ states (J/ψ and ψ'), all these states couple to open charm decay strongly, resulting in large total widths which could not be described well by the potential models [3]. Hadronic transitions play an important role in charmonium decays. Therefore, experimental study of hadronic transition will help us understand the nature of the excited charmonia.

Recently, exotic charmoniumlike states have been discovered around 4 GeV [4], which means hidden charm coupling is also prominent for new states lying in this energy region. Thus, careful investigation of hidden charm cross section is necessary and will give us a chance to clarify new charmoniumlike states. In this paper, we report the cross section measurement of $\eta J/\psi$ and $\pi^0 J/\psi$ process at $\sqrt{s} = 4.009$ GeV. In the analysis, J/ψ is reconstructed with lepton pairs.

II. BESIII/BEPCII

BESIII/BEPCII [5] is a major upgrade of BESII/BEPC [6]. The BESIII detector is designed to study hadron spectroscopy and τ-charm physics [7]. The cylindrical BESIII is composed of a Helium-gas based drift chamber (MDC), a Time-of-Flight (TOF) system, a CsI(Tl) Electro-Magnetic Calorimeter (EMC) and a RPC-based muon chamber (MUC) with a superconducting magnet providing 1.0 T magnetic field in the central region of BESIII. The expected charged particle momentum resolution and photon energy resolution are 0.5% and 2.5% at 1 GeV respectively. The photon energy resolution of BESIII is much better than that of BESII and comparable to those of CLEO [8] and Crystal Ball [9].

III. THE DATA SAMPLE AND MC SIMULATION

This analysis is finished based on a 477 pb^{-1} data sample collected with the BESIII detector operating at BEPCII at $\sqrt{s} = (4.009 \pm 0.001)$ GeV. The integrated luminosity of this data sample was measured using Bhabha events, with an estimated uncertainty of 1.1%. In order to control systematic error effectively, a small data sample with $\sim$ 7 million ψ' events was taken at $\sqrt{s} =$ 3.686 GeV under the same experimental condition.

The optimization of event selection criteria and the estimation of the backgrounds are performed through Monte Carlo (MC) simulations. The GEANT4-based simulation software BOOST [10] includes the geometric description of the BESIII detectors and the current analysis is performed in the framework of the BESIII Offline Software System-6.5.5 [11].

In order to determine detection efficiency and optimize selection criteria, we generate signal MC samples of $e^+e^- \to (\gamma_{ISR})\eta J/\psi$ and $(\gamma_{ISR})\pi^0 J/\psi$. The initial state radiation (ISR) is simulated with KKMC [12], assuming $\eta J/\psi$ and $\pi^0 J/\psi$ are produced via $\psi(4040)$ decays (using HELAMP [with 1 0 0 0 -1 0 setting] generator), and the $\psi(4040)$ is described with a Breit-Wigner (BW) function with a constant width. The maximum energy of the radiative photon is about 347 MeV and 700 MeV, corresponding to $\eta J/\psi$ and $\pi^0 J/\psi$ production threshold, respectively. J/ψ will decay to e^+e^- and $\mu^+\mu^-$ with identical branching ratio and Final State Radiation (FSR) effect associate with leptons is handled by PHOTOS.

Each MC sample for each signal mode contains 20,000 events. For the possible backgrounds study, an inclusive $\psi(4040)$ MC sample equivalent to 1 fb^{-1} integrated luminosity is also used: $\psi(4040)$ resonance, Initial State Radiation of the vector charmonium states, and QED events are generated with KKMC [12], the main known decay modes are generated with EvtGen with branching fractions being set to the world average values according to PDG [2] and the remaining events associate with charmonium decays are generated with Lundcharm [13] while other hadronic events are generated with PYTHIA [14].

IV. EVENT SELECTION CRITERIA

For $\eta J/\psi$ and $\pi^0 J/\psi$ processes, the J/ψ candidate is reconstructed with lepton pairs (i.e. e^+e^- or $\mu^+\mu^-$) and η/π^0 is reconstructed with two γs. In each candidate event of interest, there are two charged tracks with high momenta and two photons. The following event selection criteria are applied to both data and MC samples:

1. Each charged track is required to originate from the interaction point, with $V_{xy} = \sqrt{V_x^2 + V_y^2} < 1$ cm, $|V_z| < 10$ cm. Here V_x, V_y, and V_z are the x, y, and z coordinates of the point of closest approach to the run dependent interaction point, respectively. The charged track is required to lie within the polar angle region $|\cos\theta| < 0.93$.

2. A neutral cluster is considered to be a good photon candidate if the following requirements are satisfied: the deposited energy is larger than 25 MeV in the Barrel EMC ($|\cos\theta| < 0.8$) or 50 MeV in the End-cap EMC ($0.86 < |\cos\theta| < 0.92$); the angle between the cluster and the nearest charged particle is required to be larger than 20 degrees. Also we require $0 < t < 14$ [in unit of 50 ns], here t is the time information from the EMC to suppress electronic noise and energy deposits unrelated to the event.

3. The number of good charged tracks is required to be two with zero net charge. For electron candidates, we further require the E/p (EMC deposit energy over momentum) ratio value larger then 0.8 of each track; and for muon candidates, the deposit energy of each track in EMC should be less than 0.4 GeV.

   Fig. 1 shows the EMC deposit energy distribution, momentum distribution and E/p scatter plot of leptons from $\eta J/\psi$ signal MC and similarly for $\pi^0 J/\psi$ MC sample. As can be seen from these distributions, the efficiency of the E/p cut and EMC deposit energy cut is quite high ($> 99\%$).

4. The number of good photons should be two and one or two additional FSR photons are allowed which stay around leptons in a small cone (5 degrees) and whose momentum will be recovered to leptons automatically. The recoiling mass of the two photons: $M_{recoil}(\gamma\gamma) = \sqrt{(P_{c.m} - P_{\gamma 1} - P_{\gamma 2})^2}$ should be between 2.9 GeV/c^2 and 3.4 GeV/c^2 in order to identify a J/ψ candidate.

   Fig. 2 (left) shows the $\gamma\gamma$ recoil mass distribution from $\eta J/\psi$ signal MC sample and similarly for $\pi^0 J/\psi$ MC sample. We can see the efficiency is still very high ($> 99\%$) here.

   Fig. 2 (middle and right) shows the N_γ distribution from $\eta J/\psi$ signal MC sample and similarity for $\pi^0 J/\psi$ MC sample. We can see that fake photon level ($N_\gamma > 2$) is low here (about 4.3% in $\mu^+\mu^-$ mode and 4.0% in e^+e^- mode).

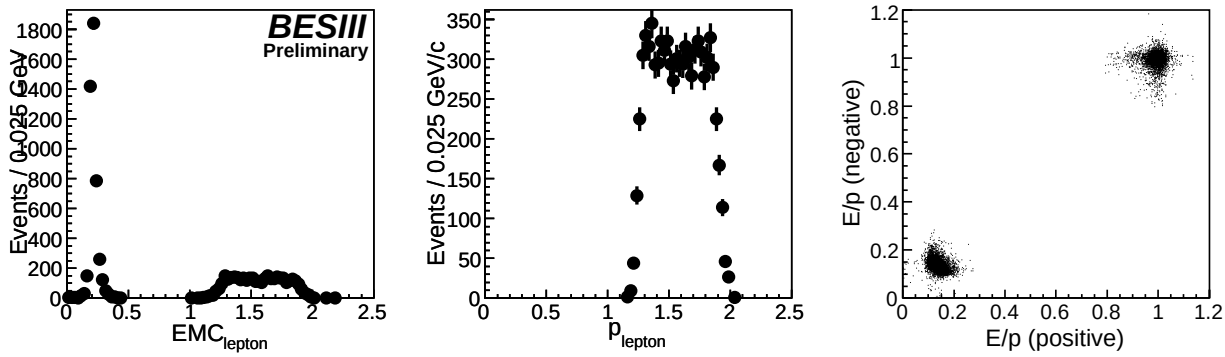

FIG. 1: (left) EMC deposit energy distribution, (middle) momentum distribution, and (right) E/p scatter plot of leptons in $\eta J/\psi$ signal MC sample. Electron events and muon events are separated clearly by EMC deposit energy and E/p ratio.

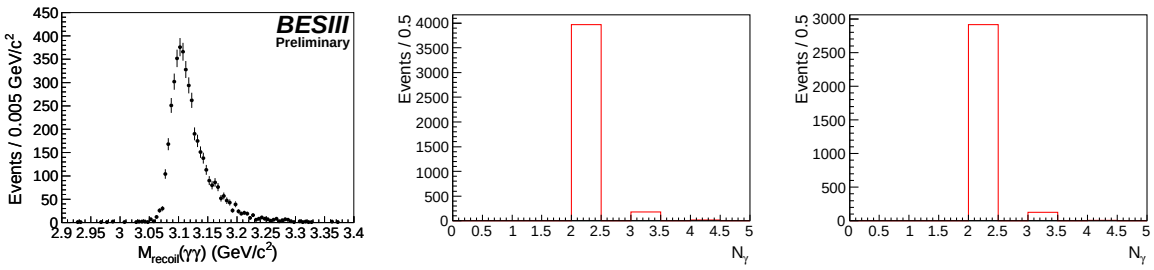

FIG. 2: $\gamma\gamma$ recoil mass distribution (left), the asymmetry tail in high mass region is due to energy leakage of photons in EMC; N_γ distribution in $\mu^+\mu^-$ mode (middle) and e^+e^- mode (right) from $\eta J/\psi$ signal MC.

5. Four-constraint (4C) kinematic fits are performed with the two charged tracks (assumed to be e^+e^- or $\mu^+\mu^-$) and the two good photon candidates and the kinematic fit chi-square is required to be less than 40 ($\chi^2 < 40$). To further separate events with one real photon and one low energy fake photon (for example $\gamma_{ISR}J/\psi$ events), three-constraint (3C) kinematic fits are also performed with the two charged tracks and two photon candidates (missing the energy of the low energy photon). In this case, the invariant mass of the $\gamma_{ISR}\ell^+\ell^-$ system would not change in kinematic fit procedure although fake photon is included.

   Fig. 3 shows the invariant mass distribution of $M(\gamma J/\psi)$ from $\gamma_{ISR}J/\psi$ MC sample. The blue histogram is from 4C fit while red histogram is from 3C fit. It's obvious that $M(\gamma J/\psi)$ from 3C fit do not change but 4C fit is lowered due to fake photon effect.

6. In order to veto $e^+e^- \to \gamma\ell^+\ell^-$ background, the invariant mass of $M(\gamma_H\ell^+\ell^-) < 3.93$ GeV/c^2 from 3C kinematic fit is required. For $\gamma_{ISR}J/\psi$ events with the ISR photon detected by EMC, since $M(\gamma_H\ell^+\ell^-)$ distribution are around 4 GeV, as can be seen from Fig. 3, so almost all of them are rejected. For QED events: $e^+e^- \to (\gamma_{ISR}...)e^+e^-/(\gamma_{ISR}...)\mu^+\mu^-$ with ISR photons detected by EMC, since the cross section of multi-photon events is highly suppressed by $\alpha \sim 1/137$, thus most of the QED events will have $\gamma\ell^+\ell^-$ final state with $M(\gamma_H\ell^+\ell^-)$ distributed around 4 GeV and would also be rejected by $M(\gamma_H\ell^+\ell^-) <$

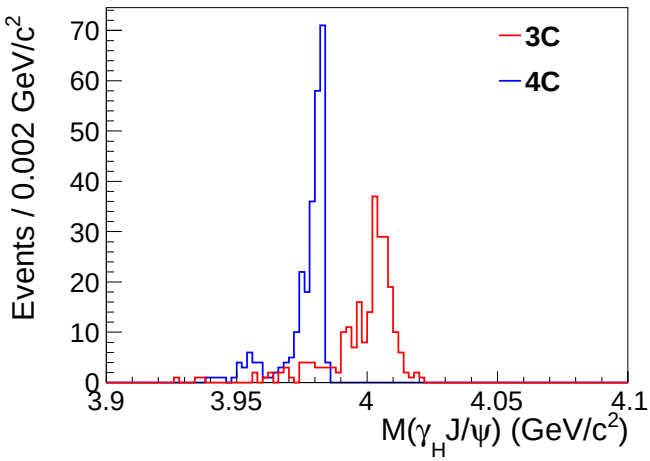

FIG. 3: The $M(\gamma J/\psi)$ mass distribution of 4C kinematic fit vs. 3C kinematic fit from $\gamma_{ISR}J/\psi$ MC sample. Mass of 4C fit is lowered due to the inclusion of one low energy fake photon but 3C fit is not affected.

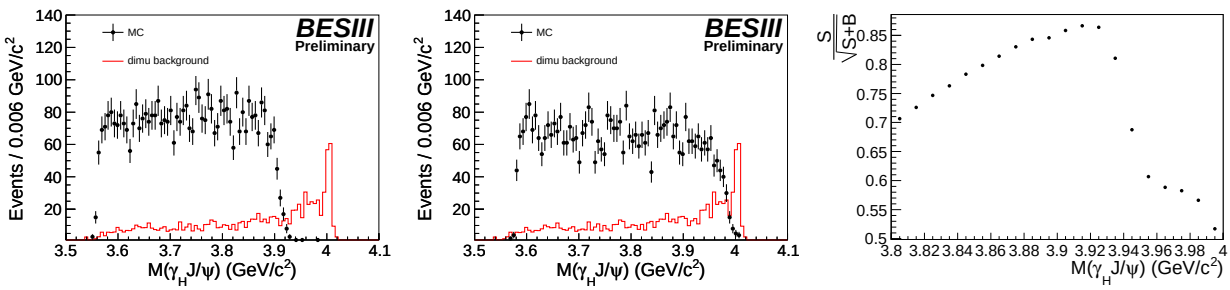

FIG. 4: (left) The $M(\gamma J/\psi)$ mass distribution of 3C kinematic fit from $\eta J/\psi$ MC sample (dots with error bars) and dimu MC sample (red histogram); (middle) from $\pi^0 J/\psi$ MC sample (dots with error bars) and dimu MC sample (red histogram); (right) $S/\sqrt{S+B}$ FOM factor vs. $M(\gamma J/\psi)$ distribution shows $M(\gamma J/\psi) < 3.93$ GeV/c^2 is optimized.

3.93 GeV/c^2 cut.

Fig. 4(left and middle) shows the $M(\gamma_H J/\psi)$ invariant mass distribution from $\eta/\pi^0 J/\psi$ signal MC and dimu MC background events. The efficiency of this cut is high ($> 99\%$) for $\eta J/\psi$ while $\sim 89\%$ for $\pi^0 J/\psi$ and will reject lots of dimu background events. Fig. 4(right) shows the optimization of $M(\gamma_H J/\psi)$ invariant mass cut using $S/\sqrt{S+B}$ as the FOM factor.

7. In order to veto $e^+e^- \to \pi^+\pi^-\pi^0$ background in $\pi^0 J/\psi$ search, we also require at least one charged track have MUC hit depth larger than 30 cm. Fig. 5 shows the scatter plot of MUC hit depth distribution for $\pi^0 J/\psi$ MC events (left), $e^+e^- \to \pi^+\pi^-\pi^0$ MC events (middle) and $\psi' \to \eta J/\psi$ data events (right). It's clear most muon tracks have large MUC hit depth (> 30 cm) while pion tracks have small MUC hit depth (< 30 cm). Hit depth less than 0 means MUC track reconstruction fails. The efficiency of this cut for signal is 87.9%

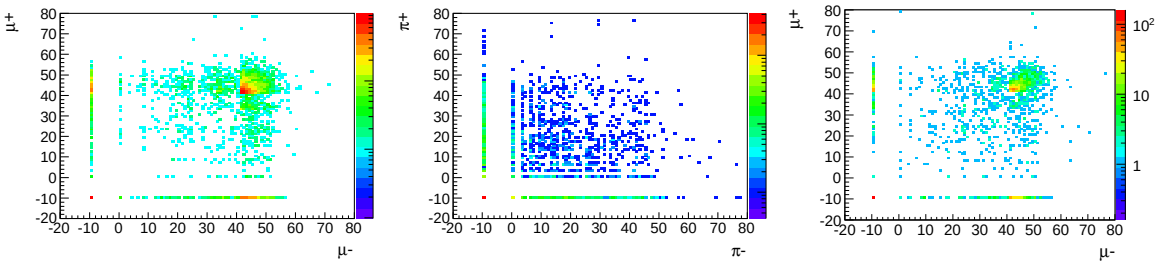

FIG. 5: Scatter plot of MUC hit depth distribution for $\pi^0 J/\psi$ MC events (left), $e^+e^- \to \pi^+\pi^-\pi^0$ MC events (middle) and $\psi' \to \eta J/\psi$ data events (right).

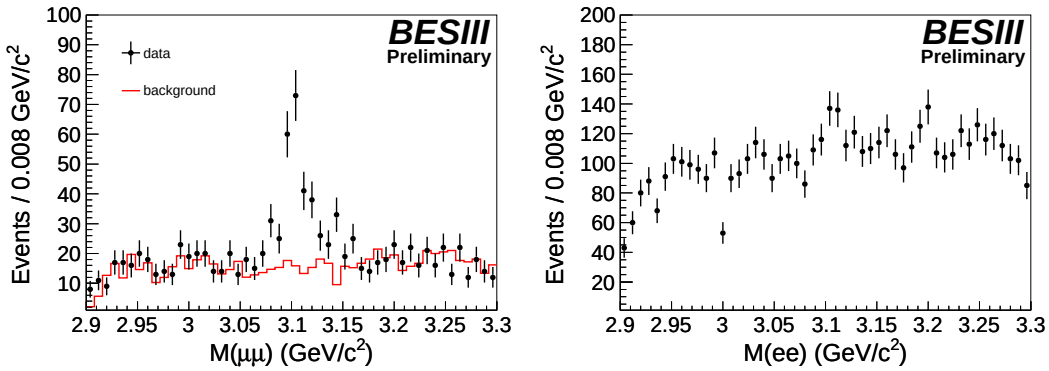

FIG. 6: (left) $M(\mu^+\mu^-)$ and (right) $M(e^+e^-)$ invariant mass distribution. Dots with error bars are data and red histogram in the left plot is inclusive MC.

(according to $\psi' \to \eta J/\psi$ data events) while about 74% background would be removed (according to $e^+e^- \to \pi^+\pi^-\pi^0$ MC events).

Since $\pi^+\pi^-\eta$ background is not significant, we do not add MUC requirement in $\eta J/\psi$ measurement.

V. DATA AND BACKGROUND ANALYSIS

After imposing all the above requirements, the invariant mass distribution of $\ell^+\ell^-$ is shown in Fig. 6, where the dots with error bars are data and the red histogram in the left plot is the sum of simulated backgrounds (normalized according to luminosity) from inclusive MC sample. Clear J/ψ signal is observed in $\mu^+\mu^-$ mode while a faint peak is also present in e^+e^- mode around 3.1 GeV. Form the left plot we can see MC simulate backgrounds well in $\mu^+\mu^-$ mode while in e^+e^- mode there are some bugs for MC sample.

In $J/\psi \to \mu^+\mu^-$ mode, the dominant background is from radiative dimu events (i.e. $e^+e^- \to \gamma\mu^+\mu^-$). This kind of background will contribute a flat distribution in $M(\ell^+\ell^-)$ invariant mass distribution as shown in Fig. 6(left). After analyzing the inclusive MC sample, we find there are still ~ 780 events left between $2.9 < M(\ell^+\ell^-) < 3.3$ GeV/c^2 region. It's impossible to eliminate such kind of background completely since they have the same final state as signal. A narrow J/ψ mass window requirement would help to suppress them. The case for $J/\psi \to e^+e^-$ mode is quite

similar. Dominant backgrounds come from radiative Bhabha events (i.e. $e^+e^- \to \gamma e^+e^-$), which would also contribute a flat distribution in $M(\ell^+\ell^-)$ invariant mass distribution. Since Bhahba cross section is about 70 times of dimu cross section at $\sqrt{s} = 4.009$ GeV, so the background level in $J/\psi \to e^+e^-$ mode is much higher than in $\mu^+\mu^-$ mode as expected in Fig. 6 (right).

Other possible background sources include $e^+e^- \to \pi^0\pi^0 J/\psi$, $\gamma\chi_{cJ}(1,2P)$, $\pi^+\pi^-\pi^0/\pi^+\pi^-\eta$. The cross section for $\pi^+\pi^- J/\psi$ at $\sqrt{s} = 4.009$ GeV is $9^{+5}_{-4} \pm 2$ pb [15]. According to isospin symmetry, the cross section of $\pi^0\pi^0 J/\psi$ should be only half of $\pi^+\pi^- J/\psi$, i.e. ~ 4.5 pb, whose contribution is negligibly small in the selected data sample according to MC simulation. For radiative transition process $\gamma\chi_{cJ}(1,2P)$, their cross sections can not be large although they are unknown. Such kind of events would not form peaking background in $M(\gamma\gamma)$ invariant mass distribution and thus will not affect our measurement by fitting $M(\gamma\gamma)$ spectrum. In fact, we also keep an eye on the search for $\gamma\chi_{cJ}(1,2P)$ process, but find no obvious evidence as discussed in Sec. VI.

The possible background of $e^+e^- \to \pi^+\pi^-\pi^0/\pi^+\pi^-\eta$ is important since it contributes absolute peaking background in $M(\gamma\gamma)$ spectrum which is used to extract number of signal events. The cross section of $\pi^+\pi^-\pi^0$ is $13.1^{+1.9}_{-1.7} \pm 2.1$ pb at $\sqrt{s} = 3.67$ GeV and $7.4 \pm 0.4 \pm 1.2$ pb at $\sqrt{s} = 3.77$ GeV [16]. The J/ψ mass sideband events are used to estimate these $\pi^+\pi^-\pi^0/\pi^+\pi^-\eta$ backgrounds.

ISR backgrounds including $\gamma_{ISR}J/\psi$, $\gamma_{ISR}\psi(2S)$ and $\gamma_{ISR}\psi(3770)$ are esitmated through inclusive MC. Only 3.3 events in $\mu^+\mu^-$ mode and 3.1 events in e^+e^- mode are found (normalized to data luminosity). As they would not peaked at either η or π^0 signal region, we neglect them in the analysis.

VI. THE FIT OF $M(\gamma\gamma)$ SPECTRUM

Fig. 7 shows fit to the $M(\ell^+\ell^-)$ invariant mass distribution of $\eta J/\psi$ MC sample with double Gaussian function, which yields a J/ψ mass of 3100.0 ± 0.8 MeV/c^2 with a resolution of 14 MeV/c^2 for lepton pairs. There is no big difference for the mass and resolution value of $\pi^0 J/\psi$ MC sample. So, the J/ψ mass window is determined to be between 3.075 GeV/c^2 and 3.125 GeV/c^2 for both modes. To reduce the uncertainty of background estimation, J/ψ mass sideband is chosen to be $2.95 < M(\ell^+\ell^-) < 3.05$ GeV/c^2 and $3.15 < M(\ell^+\ell^-) < 3.25$ GeV/c^2, which is 4 times of the signal region. The selection efficiency is 38.0% for $\eta J/\psi$ in $\mu^+\mu^-$ mode and 26.9% in e^+e^- mode. For $\pi^0 J/\psi$, the selection efficiency is 31.1% in $\mu^+\mu^-$ mode. The lower efficiency in $\pi^0 J/\psi$ mode compared to $\eta J/\psi$ is due the $M(\gamma_H\ell^+\ell^-) < 3.93$ GeV/c^2 cut and MUC cut.

After requiring $M(\ell^+\ell^-)$ lies in J/ψ mass window, Fig. 9 shows the invariant mass distribution of $M(\gamma\gamma)$ from $J/\psi \to \mu^+\mu^-$ mode (left plot) and $J/\psi \to e^+e^-$ mode (right plot). Dots with error bars are data and green shade histograms are from J/ψ mass sideband. Significant η signal is observed both in $J/\psi \to \mu^+\mu^-$ mode and $J/\psi \to e^+e^-$ mode while only a little π^0 peak is observed in $J/\psi \to \mu^+\mu^-$ mode. Further more, J/ψ mass sideband events distribution shows there are peaking π^0 background. The mass resolution is 9.0 MeV for η and 5.2 MeV for π^0 through MC simulation. In order to check the agreement between data and MC for $M(\gamma\gamma)$ mass resolution, we make use of the $\psi' \to \eta/\pi^0 J/\psi$ control sample. Fig. 8 shows the $M(\gamma\gamma)$ mass spectrum fit results from $\psi' \to \eta/\pi^0 J/\psi$ control sample using MC histogram convolving free Gaussian functions. The width of Gaussian for η convolving is (3.4 ± 0.6) MeV and for π^0 convolving is (2.4 ± 0.9) MeV in $\mu^+\mu^-$ mode and this value is (4.6 ± 0.6) MeV in e^+e^- mode for η convolving.

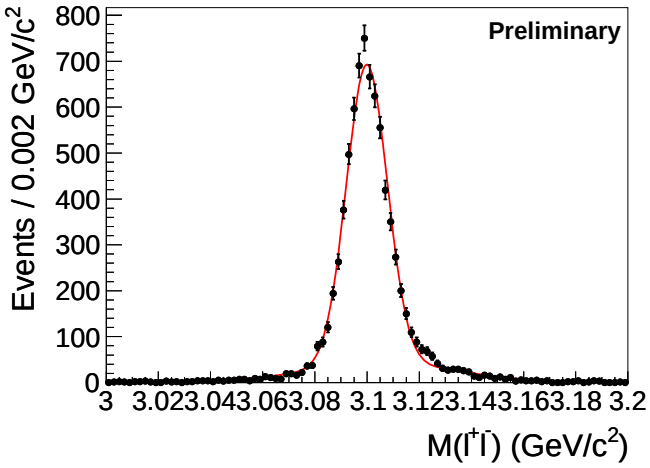

FIG. 7: Fit $M(\ell^+\ell^-)$ invariant mass distribution of $\eta J/\psi$ MC sample with double Gaussian function. The fit yields $M(J/\psi) = 3100 \pm 0.8$ MeV/c^2 with resolution $\sigma = 14$ MeV/c^2.

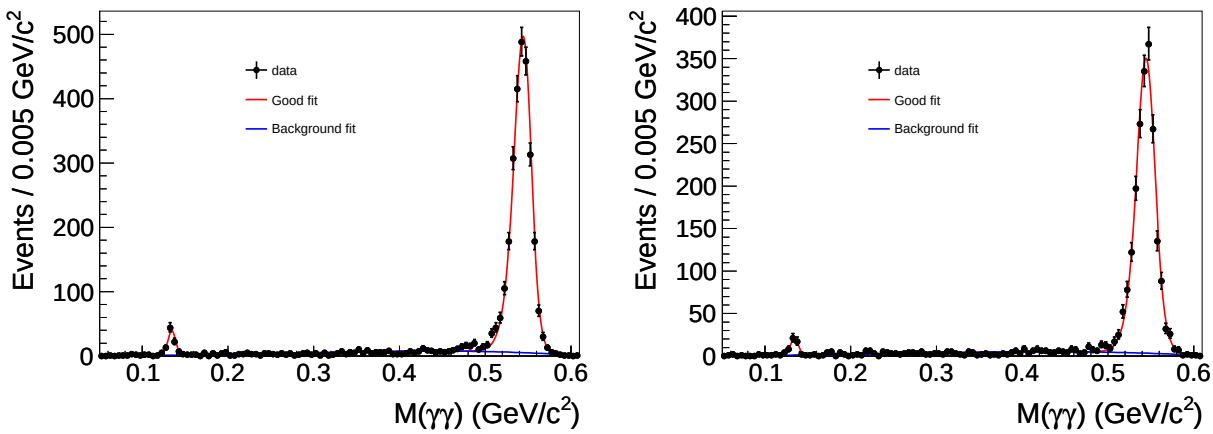

FIG. 8: Fit $M(\gamma\gamma)$ invariant mass distribution in $\mu^+\mu^-$ mode (left) and e^+e^- mode (right) for $\psi' \to \eta/\pi^0 J/\psi$ control sample with MC histogram convolving free Gaussian functions.

The $M(\gamma\gamma)$ invariant mass distributions are fitted using unbinned maximum likelihood method with MC simulated histogram convolving Gaussian function. The signal function for η is $M(\gamma\gamma)$ mass distribution from $\eta J/\psi$ MC sample and π^0 is from $\pi^0 J/\psi$ MC sample. Considering the difference between data and MC for $M(\gamma\gamma)$ resolution, two Gaussian functions were convolved to η signal and π^0 signal, respectively. For η signal, the parameters of Gaussian convolved are free while for π^0 signal, the parameter of Gaussian convolved is fixed according to the value from $\psi' \to \pi^0 J/\psi$ control sample fit result. Background shaped is described by 3rd order polynomial. The red curves in Fig. 9 show the total fit results and the blue curves show the background fit for $\mu^+\mu^-$ mode and e^+e^- mode. The fit yields

$$N(\eta)_{\mu^+\mu^-} = 111.4 \pm 11.0; \; N(\eta)_{e^+e^-} = 61.4 \pm 10.5. \tag{1}$$

The width of Gaussian functions convolved to η is (3.7 ± 1.0) MeV in $\mu^+\mu^-$ mode and (3.7 ± 1.9) MeV in e^+e^- mode. Good agreement is observed between two modes and these values agree

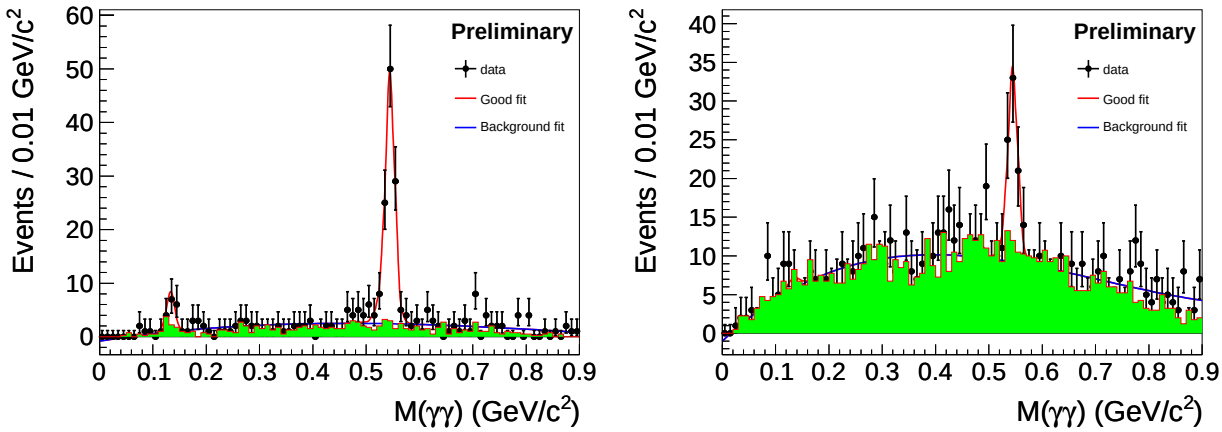

FIG. 9: (left) $M(\gamma\gamma)$ invariant mass distribution from $J/\psi \to \mu^+\mu^-$ mode and (right) from $J/\psi \to e^+e^-$ mode when $M(\ell^+\ell^-)$ lies in J/ψ mass window. Dots with error bars are data and green shaded histograms are normalized $M(\gamma\gamma)$ distribution when $M(\ell^+\ell^-)$ lies in J/ψ mass sideband. The red curves show the total fit using MC histogram of $M(\gamma\gamma)$ mass distribution from $\eta J/\psi$ MC sample and $\pi^0 J/\psi$ MC sample convolving Gaussian as signal function and blue curves show the background fit using 3rd order polynomial.

with results from $\psi' \to \eta J/\psi$ control sample reasonable well.

To estimate goodness of the fit, the χ^2 test method is used which gives $\chi^2/n.d.f = 14.1/14 = 1.0$ for $\mu^+\mu^-$ mode and $\chi^2/n.d.f = 42.9/43 = 1.0$ for e^+e^- mode. These indicate that the fit quality is quite good.

The peaking π^0 background in $J/\psi \to \mu^+\mu^-$ mode is estimated through J/ψ mass sideband events. Fig. 10 shows the $M(\gamma\gamma)$ invariant mass distribution from J/ψ mass sideband region (left) and signal region (right) after applying MUC cut in $\mu^+\mu^-$ mode. Dots with error bars are data and red histogram in left plot is from inclusive MC sample. We can see a quite clear π^0 peak which comes from $\pi^+\pi^-\pi^0$ process. Inclusive MC sample does not show π^0 peak there because such kind of process is not simulated well by PYTHIA [14]. A fit using Gaussian function as signal pdf yields $N(\pi^0)^{\rm SB} = 11.3 \pm 4.4$ events. Thus, the normalized peaking π^0 background is calculated to be $N(\pi^0)^{\rm bkg} = 2.8 \pm 1.1$ events.

In order to estimate the statistical significance of π^0 signal, we fix the number of signal events to 0 and obtain the log-likelihood value ($\ln \mathcal{L}_0$). The statistical significance is estimated through the difference of the logarithmic likelihoods, i.e. $-2\ln(\mathcal{L}_0/\mathcal{L}_{max})$, taking the difference in the number of degrees of freedom (Δndf) in the fit into account, where $\mathcal{L}_{max}$ is the likelihood value of the best fit. The value for π^0 signal is estimated to be 1.1σ here, which means $\pi^0 J/\psi$ production at $\sqrt{s} = 4.009$ GeV is not significant. Thus, we give an upper limit estimation for $\pi^0 J/\psi$ production. Fit the $M(\gamma\gamma)$ invariant mass distribution after applying MUC cut as shown in Fig. 10 (right), we get $N(\pi^0)^{\rm tot}$ <11.7 at 90% C.L. Considering the peaking background estimated from J/ψ mass sideband, we have $N(\pi^0)^{\rm signal} < 8.9$ at 90% C.L.

In the $\gamma\gamma J/\psi$ final state, we can also investigate the $M(\gamma J/\psi)$ mass spectrum aiming at searching for $e^+e^- \to \gamma\chi_{cJ}(1,2P)$ production. Fig. 11 shows the $M(\gamma J/\psi)$ (two entries per event) invariant mass distribution from $J/\psi \to \mu^+\mu^-$ mode. Dots with error bars are data and red histogram is inclusive MC simulated background. The contribution from $\eta J/\psi$ and $\pi^0 J/\psi$ backgrounds is added to the inclusive MC sample according to the measurement present in this analysis. The small bump in Fig. 11 at around 3.52 GeV/c^2 may suggest a χ_{c1} signal, a fit with MC his-

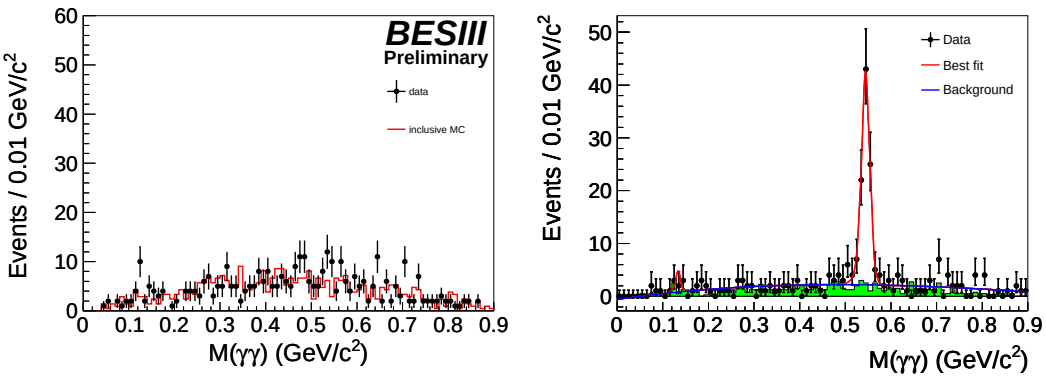

FIG. 10: $M(\gamma\gamma)$ invariant mass distribution (un-normalized) from J/ψ mass sideband region (left) and signal region (right) with MUC requirement. Dots with error bars are data and red histogram in the left plot is inclusive MC.

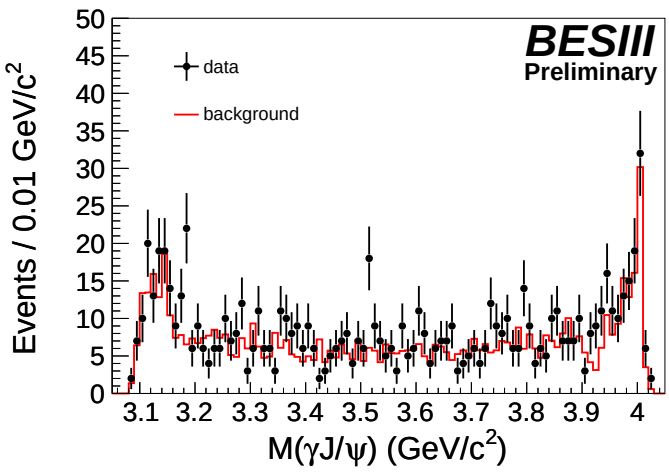

FIG. 11: $M(\gamma J/\psi)$ invariant mass distribution from kinematic fit 3C in $J/\psi \to \mu^+\mu^-$ mode. Dots with error bars are data and red histogram is inclusive MC background. Here $\eta J/\psi$ and $\pi^0 J/\psi$ backgrounds have been added to inclusive MC according to this measurement.

togram convolving Gaussian yields $\mathrm{N}(\chi_{c1}) = 15.9 \pm 6.1$ events. The MC simulation indicates the selection efficiency for $\gamma\chi_{c1}$ is 41.8% while the mass resolution is about 12 MeV/c^2 for χ_{c1} signal. We measures the observed cross section $\sigma(e^+e^- \to \gamma\chi_{c1}) = 3.73 \pm 1.43$ pb at $\sqrt{s} = 4.009$ GeV and the upper limits < 6.8 pb at the 90% confidence level. The statistical significance is estimated to be $< 3.1\sigma$ for $\gamma\chi_{c1}$ production.

With current statistics and backgrounds level, we can not conclude any significant evidence for the existence of $e^+e^- \to \gamma\chi_{cJ}(1,2P)$ production. As for $J/\psi \to e^+e^-$ mode, since signal yields is the same but background level is $\sim$ 70 times more than in $\mu^+\mu^-$ mode, the situation for $\gamma\chi_{cJ}(1,2P)$ search is even worse and we do not show the plot here. No signal for the $\gamma\chi_{cJ}(1,2P) \to \gamma\gamma J/\psi$ events in our data also indicates that such kind of background contamination in our $\eta J/\psi$ and $\pi^0 J/\psi$ measurement is negligible.

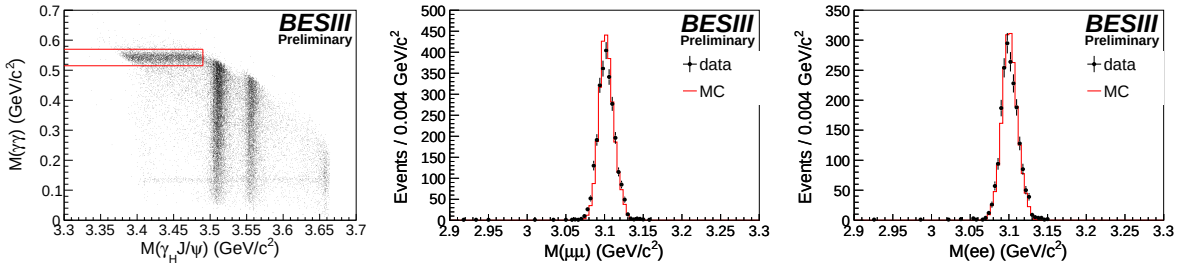

FIG. 12: (left) Scatter plot of $M(\gamma\gamma)$ vs. $M(\gamma J/\psi)$ invariant mass distribution from ψ' on-resonance data sample. The red box shows $\eta J/\psi$ events distribution. (middle) $M(\mu^+\mu^-)$ and (right) $M(e^+e^-)$ invariant mass distribution from selected $\eta J/\psi$ data sample. Dots with error bars are data and red histograms are from MC simulation.

VII. SYSTEMATIC ERROR ESTIMATION

A. Lepton pair mass resolution

The systematic error associated with lepton pair invariant mass resolution is estimated using the ψ' on-resonance data sample taken in company with the $\sqrt{s} = 4.009$ GeV data sample. The same selection criteria were performed and we can get $\eta J/\psi$, $\pi^0 J/\psi$ and $\gamma\chi_{c0,1,2}$ sub-samples. Fig. 12(left) shows the scatter plot of $M(\gamma\gamma)$ vs. $M(\gamma_H J/\psi)$, where we can see clear η/π^0 signal in $M(\gamma\gamma)$ invariant mass distribution and $\chi_{c1,2}$ signal in $M(\gamma J/\psi)$ invariant mass distribution. The band of χ_{c0} signal also can be seen on the left most side of the plot. Besides these, there are $\pi^0\pi^0 J/\psi$ background events in the scatter plot.

Requiring $0.515 < M(\gamma\gamma) < 0.57$ GeV/c^2 and $M(\gamma J/\psi) < 3.49$ GeV/c^2 (as the red box shows), we can obtain a clean $\eta J/\psi$ data sample with purity about 98.5% in $\mu^+\mu^-$ mode and 98.3% in e^+e^- mode. Fig. 12(middle) and (right) show the lepton pair invariant mass distribution from this selected $\eta J/\psi$ data sample. Dots with error bars are data and red histograms are MC simulation. So, the efficiency of the J/ψ mass window cut (i.e. $3.075 < M(\ell^+\ell^-) < 3.125$ GeV/c^2) is 0.968 ± 0.003 for data and 0.983 ± 0.001 for MC simulation in $\mu^+\mu^-$ mode and 0.960 ± 0.005 for data and 0.983 ± 0.001 for MC simulation in e^+e^- mode. Thus, the systematic error is calculated to be 1.53% for $\mu^+\mu^-$ mode and 2.34% for e^+e^- mode.

B. Kinematic fit

For kinematic fit, the helix parameters smearing method of leptons is involved for MC simulation. The same $\psi' \to \eta J/\psi$ control sample as described above is used to investigate systematic error due to kinematic fit. Fig. 13 shows the χ^2 distribution from $\mu^+\mu^-$ mode and e^+e^- mode, respectively. We can see data agree with MC well. The efficiency difference between data and MC is 1.9% both in $\mu^+\mu^-$ mode and e^+e^- mode for $\chi^2 < 40$, which is taken as systematic error from kinematic fit.

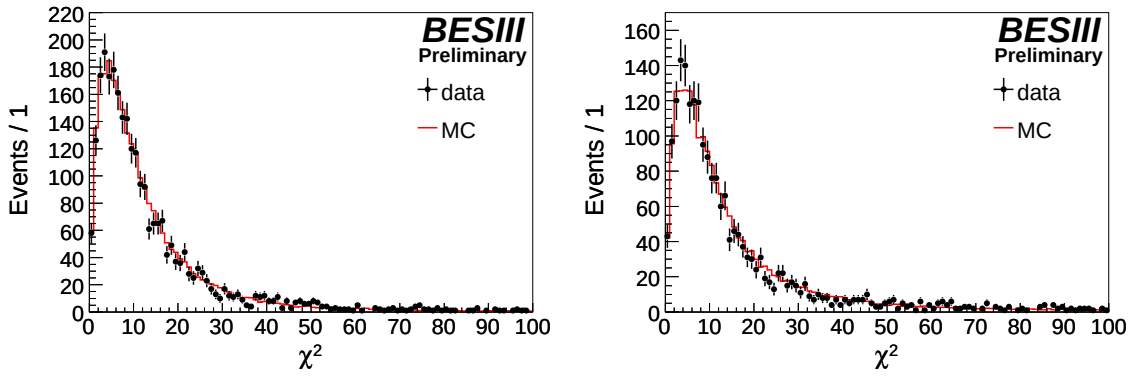

FIG. 13: χ^2 distribution of Kinematic fit 4C for $\mu^+\mu^-$ mode (left) and e^+e^- mode (right) in $\psi' \to \eta J/\psi$ on-resonance data sample. Dots with error bars are data and red histograms are MC simulation of the signal events.

C. Background shape

The systematic uncertainty from background shape is estimated through varying the background shape from 3rd order polynomial to 2nd order or 4th order and the difference is 1.5% in $\mu^+\mu^-$ mode and 3.0% in e^+e^- mode for $\eta J/\psi$. For $\pi^0 J/\psi$, the uncertainty from background shape is mainly due to peaking background estimation, which gives 9.4% in $\mu^+\mu^-$ mode.

D. Resonance parameters and $\psi(4040)$ line shape

The initial state radiation is simulated with KKMC, assuming the $e^+e^- \to \eta J/\psi$ and $\pi^0 J/\psi$ are produced via $\psi(4040)$ decays. The uncertainty of $\psi(4040)$ resonance parameters would introduce uncertainty to the radiative correction factor and efficiency. Changing the BW parameters (mass and width) according to PDG values [2] results in a variation of $(1+\delta)\times\epsilon$ of 1.5% in $\mu^+\mu^-$ mode and 1.0% in e^+e^- mode for $\eta J/\psi$ and 2.6% in $\mu^+\mu^-$ mode for $\pi^0 J/\psi$.

The possible distortion of the $\psi(4040)$ resonance line shape due to the interference effect with the nearby $\psi(4160)$ resonance would also introduce uncertainty in the radiative correction factor and efficiency. Following the result listed in Ref. [18], the difference in $(1+\delta)\times\epsilon$ is 1.3% in $\mu^+\mu^-$ mode and 3.1% in e^+e^- mode for $\eta J/\psi$, and 3.0% in $\mu^+\mu^-$ mode for $\pi^0 J/\psi$. They are taken as systematic errors due to $\psi(4040)$ line shape.

E. Branching ratio of intermediate state decays and others

The systematic error from $\mathcal{B}(J/\psi \to \ell^+\ell^-)$ is taken as 1% and from $\mathcal{B}(\eta \to \gamma\gamma)$ is taken as 0.5% [2].

Systematic uncertainty of integrate luminosity is 1.1% through a measurement from $e^+e^- \to e^+e^-$ events production. For track finding, 1% per track is generally accepted at BESIII and for photon detection, 1% per photon is also generally used at BESIII. Since we used $e^+e^- \to e^+e^-$ events to measure luminosity, so the track finding error for e^+e^- is canceled out automatically.

The final state radiation (FSR) was handled with PHOTOS and was tested with pure $\psi' \to$

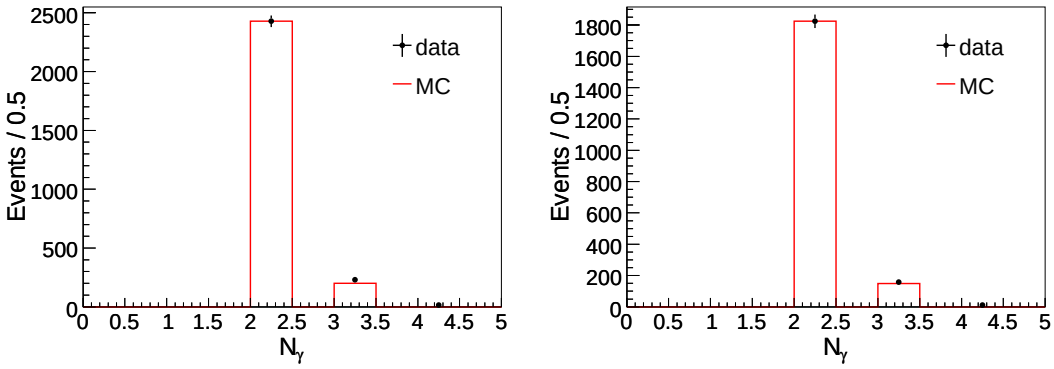

FIG. 14: N_γ distribution in $\mu^+\mu^-$ mode (left) and e^+e^- mode (right) for $\psi' \to \eta J/\psi$ on-resonance data sample. Dots with error bars are data and red histogram are signal MC events.

$\pi^+\pi^- J/\psi$ data events. It is found that MC simulates data very well (within 5%). Considering FSR events only contribute a small fraction ($\sim$7% for $\mu^+\mu^-$ mode and $\sim$20% for e^+e^- mode), so its systematic uncertainty is estimated to be small. Since FSR effect only affect lepton pair invariant mass distribution and kinematic fit efficiency, so its systematic uncertainty has been included already.

Systematic uncertainty from fake photon simulation is estimated by using the selected $\psi' \to \eta J/\psi$ control sample. Fig. 14 shows the N_γ distribution in $\mu^+\mu^-$ mode and e^+e^- mode, respectively. It's obvious that MC simulate data quite well and the systematic error due to photon number cut is conservatively estimated to be 1%.

Other sources including E/p ratio cut for electrons, EMC deposit energy cut for muons and so on. All these cuts have efficiency higher than 99%, their contribution are small and are neglected.

F. Total systematic error

The systematic error sources and their contributions are summarized in Table I for $\eta J/\psi$ and $\pi^0 J/\psi$, respectively. The total systematic for $\eta J/\psi$ in $\mu^+\mu^-$ mode is estimated to be 5.0%, while 6.1% in e^+e^- mode. For $\pi^0 J/\psi$, total systematic is estimated to be 11.1% in $\mu^+\mu^-$ mode.

VIII. RESULTS AND DISCUSSION

The Born-order cross section is calculated using the following formulism:

$$\sigma^B = \frac{N^{obs}}{\mathcal{L}_{int}(1+\delta)\epsilon\mathcal{B}} \tag{2}$$

where N^{obs} is the number of observed events, $\mathcal{L}_{int}$ is integrate luminosity, ϵ is selection efficiency, $\mathcal{B}$ is branching ratio of intermediate states and (1+δ) is the radiative correction factor, which is defined as below:

$$(1+\delta) = \frac{\sigma^{obs}}{\sigma^B} = \frac{\int \mathrm{BW}(s(1-x))F(x,s)dx}{\mathrm{BW}(s)} \tag{3}$$

TABLE I: Summary of the systematic errors (%) in $\mu^+\mu^-$ mode and e^+e^- mode.

Source	$\eta\mu^+\mu^-$	ηe^+e^-	$\pi^0\mu^+\mu^-$
Luminosity	1.1	1.1	1.1
Track finding	2	-	2
Photon detection	2	2	2
Lepton pair mass resolution	1.6	2.4	1.6
Kinematic fit	1.9	1.9	1.9
Background shape	1.5	3.0	9.4
$\psi(4040)$ parameters and line shape	2.0	3.3	4.0
Branching ratios	1.2	1.2	1.0
Others	1.0	1.0	1.0
Total	5.0	6.1	11.1

Here, $F(x,s)$ is radiator function, which is from QED calculation [17] with accuracy 0.1%; and BW(s) is Breit-Wigner shape of the $\psi(4040)$ resonance with constant total width [2]. We make an assumption that all $\eta/\pi^0 J/\psi$ events are from $\psi(4040)$ decay. The output value for (1+δ) is 0.757 ± 0.003 from KKMC, which is in good agreement with QED calculation [17].

For $\eta J/\psi$ process, the cross section in $\mu^+\mu^-$ mode is measured to be

$$\sigma^B_{\mu^+\mu^-}(\eta J/\psi) = 34.8 \pm 3.5 \pm 1.8 \text{ pb}, \tag{4}$$

while in e^+e^- mode is

$$\sigma^B_{e^+e^-}(\eta J/\psi) = 27.1 \pm 4.7 \pm 1.7 \text{ pb}. \tag{5}$$

Here the first errors are statistical and the second ones systematic.

As the measurement from the two modes are consistent with each other, we take an weighted average for the final result, the common systematic error in these two measurement are handled properly in doing the average. We obtain, at $\sqrt{s} = 4.009$ GeV,

$$\sigma^B(e^+e^- \to \eta J/\psi) = 32.1 \pm 2.8 \pm 1.3 \text{ pb}. \tag{6}$$

As the significance for the $\pi^0 J/\psi$ signal is low, we give the upper limit on the production cross section at the 90% confidence level. By lowering the efficiency by a factor of $(1-\sigma_{\text{sys}})$, we obtain, at $\sqrt{s} = 4.009$ GeV,

$$\sigma^B(\pi^0 J/\psi) < 1.5 \text{ pb}. \tag{7}$$

All these measurements do not contradict with the upper limits set by the CLEO experiment [15].

The cross section of $e^+e^- \to \eta J/\psi$ at $\sqrt{s} = 4.009$ GeV is the first measurement. If we assume it is from $\psi(4040)$ transition, by using the total cross section of $\psi(4040)$ at 4.009 GeV [(6.2 ± 0.6) nb] calculated with the PDG [2] values of the resonant parameters as input, we get

$$\mathcal{B}(\psi(4040) \to \eta J/\psi) = (5.2 \pm 0.5 \pm 0.2 \pm 0.5) \times 10^{-3}, \tag{8}$$

where the first, the second, and the third errors are statistical, systematic, and the uncertainty from the $\psi(4040)$ parameters. This is the first measurement of this quantity. It is much large than the same transition of the $\psi(3770)$ and also more than two times of the transition ratio for $\psi(4040) \to \pi^+\pi^- J/\psi$.

With the same method, we can determine

$$\mathcal{B}(\psi(4040) \to \pi^0 J/\psi) < 0.26 \times 10^{-3}, \tag{9}$$

at the 90% confidence level. Here the uncertainty from the $\psi(4040)$ parameters has also been considered.

---

[1] J. Siegrist *et al.*, Phys. Rev. Lett. **36**, 700 (1976).

[2] K. Nakamura *et al.*, (Particle Data Group), J. Phys. G **37**, 075021 (2010).

[3] E. Eichten *et al.*, Phys. Rev. D **17**, 3090 (1978); **21**, 203 (1980); T. Barnes, S. Godfrey, and E. S. Swanson, Phys. Rev. D **72**, 054026 (2005).

[4] B. Aubert *et al.* (*BABAR* Collaboration), Phys. Rev. Lett. **95**, 142001 (2005); C. Z. Yuan *et al.* (Belle Collaboration), Phys. Rev. Lett. **99**, 182004 (2007).

[5] M. Ablikim *et al.* (BESIII Collaboration), Nucl. Instrum. Methods Phys. Res., Sect. A **614**, 345 (2010).

[6] J. Z. Bai *et al.* (BES Collaboration), Nucl. Instr. and Meth. Phys. Res. Sect. A **344**, 319 (1994); **458**, 627 (2001).

[7] D. M. Asner *et al.*, Int. J. Mod. Phys. A **24**, 499 (2009).

[8] G. Viehhausser *et al.*, Nucl. Instr. Meth. A **462**, 146 (2001).

[9] M. Oreglia *et al.*, Phys. Rev. D **25**, 2559 (1982).

[10] Z. Y. Deng *et al.*, High Energy Phys. Nucl. Phys. **30**, 371 (2006).

[11] W. D. Li, H. M. Liu *et al.*, in proceeding of CHEP06, Mumbai, India, 2006 edited by Sunanda Banerjee (Tata Institute of Fundamental Research , Mumbai, 2006).

[12] S. Jadach, B. F. L. Ward, and Z. Was, Comput. Phys. Commun. **130**, 260 (2000); Phys. Rev. D **63**, 113009 (2001).

[13] R. G. PING *et al.*, Chinese Phys. C **32**, 599 (2008).

[14] http://home.thep.lu.se/∼torbjorn/Pythia.html

[15] T. E. Coan *et al.* (CLEO Collaboration), Phys. Rev. Lett. **96**, 162003 (2006).

[16] G. S. Adams *et al.* (CLEO Collaboration), Phys. Rev. D **73**, 012002 (2006).

[17] E. A. Kuraev and V. S. Fadin, Yad. Fiz. **41**, 733-742 (1985).

[18] X. L. Wang for the Belle Collaboration, talk at the FPCP meeting [http://hepg-work.ustc.edu.cn/fpcp2012].